

Research Article

Open Access



Influence of softening annealing on microstructural heredity and mechanical properties of medium-Mn steel

Fanglin Ding^{1#}, Qinyi Guo^{1#}, Bin Hu¹, Haiwen Luo¹

¹Department of Ferrous Metallurgy, University of Science and Technology Beijing, Beijing 100083, China.

[#]Authors contributed equally.

Correspondence to: Prof. Haiwen Luo, Department of Ferrous Metallurgy, University of Science and Technology Beijing, 30 Xueyuan Road, Haidian District, Beijing 100083, China. E-mail: luohaiwen@ustb.edu.cn; Dr. Bin Hu, Department of Ferrous Metallurgy, University of Science and Technology Beijing, 30 Xueyuan Road, Haidian District, Beijing 100083, China. E-mail: hubin@ustb.edu.cn

How to cite this article: Ding F, Guo Q, Hu B, Luo H. Influence of softening annealing on microstructural heredity and mechanical properties of medium-Mn steel. *Microstructures* 2022;2:2022009. <https://dx.doi.org/10.20517/microstructures.2022.01>

Received: 16 Jan 2022 **First Decision:** 10 Feb 2022 **Revised:** 21 Feb 2022 **Accepted:** 21 Mar 2022 **Published:** 29 Mar 2022

Academic Editors: Zibin Chen, Shujun Zhang **Copy Editor:** Jia-Xin Zhang **Production Editor:** Jia-Xin Zhang

Abstract

Softening annealing (SA) is often required for producing medium-Mn steels (MMS) as it lowers hardness so that they can be cold rolled to reduce thickness. The influences of different SA processes on the microstructural heredity during the processing route and the final tensile properties were studied. It was found that the SA process could either intensify or weaken the influence of the Mn segregation resulting from solidification on the subsequent microstructural evolution during the process, *i.e.*, microstructural heredity. In the case when no SA was employed, both recrystallization and rapid growth of ferrite grains preceded the reverse austenitic transformation during the intercritical annealing (IA) in the Mn-lean regions, where very coarse ferrite grains were formed. This deteriorated ductility due to the propagation of cracking along the boundary of the coarse-grained and fine-grained regions. In contrast, SA at a sufficiently high temperature could dissolve cementite, producing uniformly distributed austenite grains. They transformed to martensite during cold rolling but were reborn during IA. As a result, ultrafine austenite and ferrite grains were uniformly distributed, which improved ductility significantly. This study hints at a new approach to altering the microstructural heredity resulting from the heterogeneous Mn distribution in MMS.

Keywords: Medium-Mn steels, intercritical annealing, Mn segregation, recrystallization, mechanical properties



© The Author(s) 2022. **Open Access** This article is licensed under a Creative Commons Attribution 4.0 International License (<https://creativecommons.org/licenses/by/4.0/>), which permits unrestricted use, sharing, adaptation, distribution and reproduction in any medium or format, for any purpose, even commercially, as long as you give appropriate credit to the original author(s) and the source, provide a link to the Creative Commons license, and indicate if changes were made.



INTRODUCTION

Recently, medium-Mn steels (MMS) (4-12 wt.% Mn content) have attracted a great attention in both industries and academia due to their reasonable alloying costs and excellent mechanical properties^[1-4]. The latter is intimately related to the metastable austenite, which is formed by the intercritical annealing (IA) process and then retained at ambient temperature. These austenite grains could transform to martensite during deformation, contributing to work hardening via the transformation-induced- plasticity effect; consequently, necking is delayed, and both plasticity and strength increase^[5,6].

The phase fraction and stability of retained austenite (RA) in MMS are usually tailored via adjusting the IA parameters, including the heating rate^[7], temperature, and duration^[8-12]. However, prior to IA, the MMS sheets may be subjected to hot forging, hot rolling (HR), cold rolling (CR), etc. All of them would change the initial microstructure for the reverse austenitic transformation. Particularly, the microstructure in the MMS after HR is often martensite having high hardness^[13], which is frequently cracked during CR; therefore, an additional softening annealing (SA) process is required to reduce the hardness for successfully realizing CR^[14]. In general, there are two types of SA processes. One is to transform the hard martensite to a softer dual-phase microstructure that consists of ferrite and austenite during the SA process above the cementite solution temperature^[15]. The other is the SA process performed below the cementite solution temperature, during which the C content in the matrix decreases due to the precipitation of cementite and dislocation density is lowered due to recovery or even recrystallization^[16].

The different initial microstructures before the reverse austenitic transformation occurring during the IA could significantly affect the resultant austenitic feature and final mechanical properties^[17]. For example, Luo *et al.*^[18] found that the as-quenched martensitic microstructure in a 5 wt.% Mn steel before the IA led to finer austenite grains and smaller Lüders strain than the cold-rolled microstructures. Ding *et al.*^[19] discovered that the pre-existing austenite fraction had a remarkable influence on both the reverse transformation kinetics and the resultant mechanical properties of Fe-0.2C-8Mn-2Al (wt.%) steel. One may note that almost all the studies focused on the initial microstructures that were not cold rolled but directly austenitized during the IA. However, cold rolling is usually necessary to reduce the thickness of automotive steel sheets. In this case, a high density of defects such as dislocations developed during cold rolling could strongly affect recrystallization and the reverse transformation kinetics during the subsequent IA; both are influenced even by the microstructures before cold rolling due to the microstructural heredity. In other words, the practical window of tailoring the starting microstructures for austenite reversion is not only in the cold-rolled process but also in the preceding SA process. Therefore, understanding the microstructural heredity during the hot rolling, softening annealing, cold rolling, and the final intercritical annealing processing stages is important for improving mechanical properties.

In this study, an MMS was first subjected to different SA processes, and then to the same CR and IA processes. The microstructural evolution during these manufacturing processes was systematically investigated and compared, and their effects on the final mechanical properties were also examined and analyzed.

MATERIALS AND METHODS

Materials preparation

The ingot with a nominal composition of Fe-5Mn-2Al-0.1C (wt.%) was cast using a vacuum induction furnace. The raw materials for smelting included pure iron (Fe \geq 99.99 wt.%), electrolytic manganese (Mn \geq 99.88 wt.%), highly pure carbon (C \sim 100 wt.%), and pure aluminum (Al \geq 99.9 wt.%). The composition of the ingot was measured by wet chemical analysis and is Fe-4.89Mn-1.96Al-0.11C (wt.%). The ingot was hot

forged into a slab with 60 mm thickness. The slab was homogenized at 1200 °C for 2 h and then hot rolled to 4.5 mm thickness plate by eight passes, about 28% reduction per pass, before oil-quenching to ambient temperature. Continuous hot rolling was used in this experiment without inter-annealing processes, and the true strain during the process was about 2.6.

Heat treatment

The equilibrium fractions of each phase in the studied steel were calculated by Thermo-Calc software with TCFE9 database, as shown in [Figure 1A](#). The results show that cementite and ferrite phases disappear at 629 and 930 °C, respectively. To explore the influences of two different microstructural origins on the final microstructures and the resultant mechanical properties, the SA temperatures were deliberately selected as the intercritical temperature of 700 °C between A_1 and A_3 and the ferritic temperature of 550 °C well below the cementite solution temperature, at which the corresponding equilibrium microstructures consist of ferrite plus 29.3% austenite and ferrite plus 1.3% cementite, respectively.

The hot-rolled plate was cut into three pieces with the dimension of $45 \times 155 \times 4.5 \text{ mm}^3$. One was directly cold rolled without being softening annealed; two were subjected to the SA at 700 °C for 10 min and 550 °C for 3 h, respectively. Since the phase transformation at 700 °C should proceed much more rapidly than that at 550 °C due to faster diffusion of solutes, a shorter SA holding duration is adopted to avoid excessive grain growth. For convenience, they are termed as WSA, SA700, and SA550, respectively. After pickling to remove the oxide layer on the surface, all steel sheets were cold rolled to 1.5 mm thickness. The total true strain during the cold rolling was about 1.1. They were then subjected to IA at 700 °C for 10 min. The above processing route is also shown in [Figure 1B](#).

Microstructure characterization

Microstructures were observed by field emission scanning electron microscopy (FE-SEM, JSM-6710F) and energy dispersive spectrometer. The IAed microstructures were particularly examined by electron backscattering diffraction (EBSD, Scanning Auger Nanoprobe, PHI 710) at the operating voltage of 20 kV with the step size of 0.08 μm . The retained austenite fraction was measured by X-ray diffraction (XRD) using Co-K_α radiation with the scanning step size of 0.02° and then calculated from the integrated intensities of the $(200)_\gamma$, $(220)_\gamma$, $(311)_\gamma$, $(200)_\alpha$, and $(211)_\alpha$ diffraction peaks^[20]. The EBSD and XRD samples were electrolytically polished for ~15 s in a mixed solution with 20% perchloric acid and 80% ethanol (vol.%) at a voltage of 20 V for examination. Electron probe microanalysis was carried out to investigate the Mn concentration distribution.

Mechanical property tests

The tensile samples were machined into a dog-bone shape along the rolling direction with a gauge length of 25 mm and a gauge width of 6 mm. Tensile deformation tests were carried out using a WDW-200C tensile testing machine at ambient temperature and a crosshead speed of 1 mm/min, *i.e.*, a strain rate of 0.0007 s^{-1} . The strain was determined by an extensometer. Two tests were repeated for each specimen, and the tensile properties were reported as the average values.

RESULTS AND DISCUSSION

[Figure 2](#) shows the SEM images and the XRD spectra on the three samples subjected to the different SA processes. The WSA sample exhibits a fully martensitic microstructure without retained austenite [[Figure 2A](#)], where martensite blocks have uneven sizes. [Figure 2B](#) and [D](#) indicate the microstructure in the SA700 sample is composed of ferrite and austenite phases. The latter has a volume fraction of ~23.7%, which is slightly lower than the equilibrium value (29.3%) predicted by Thermo-Calc. SA550 is composed of ferrite as the matrix and cementite that was formed at the high angle boundaries [[Figure 2C](#)]. Note that the ferrite

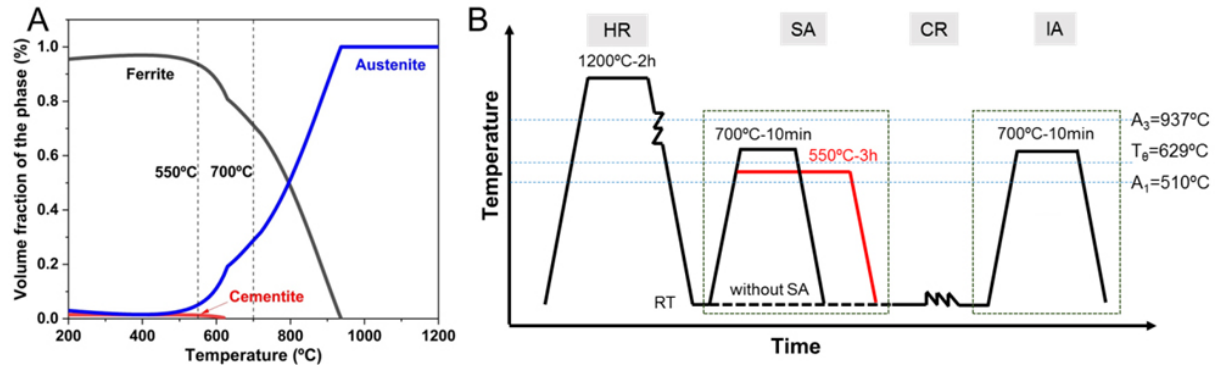


Figure 1. (A) The equilibrium phase fraction calculated by Thermo-Calc software. (B) Schematic diagram of the processing route used in the present study. A_1 , A_3 , and T_0 are the equilibrium temperatures of austenite formation and disappearance and cementite solution, respectively.

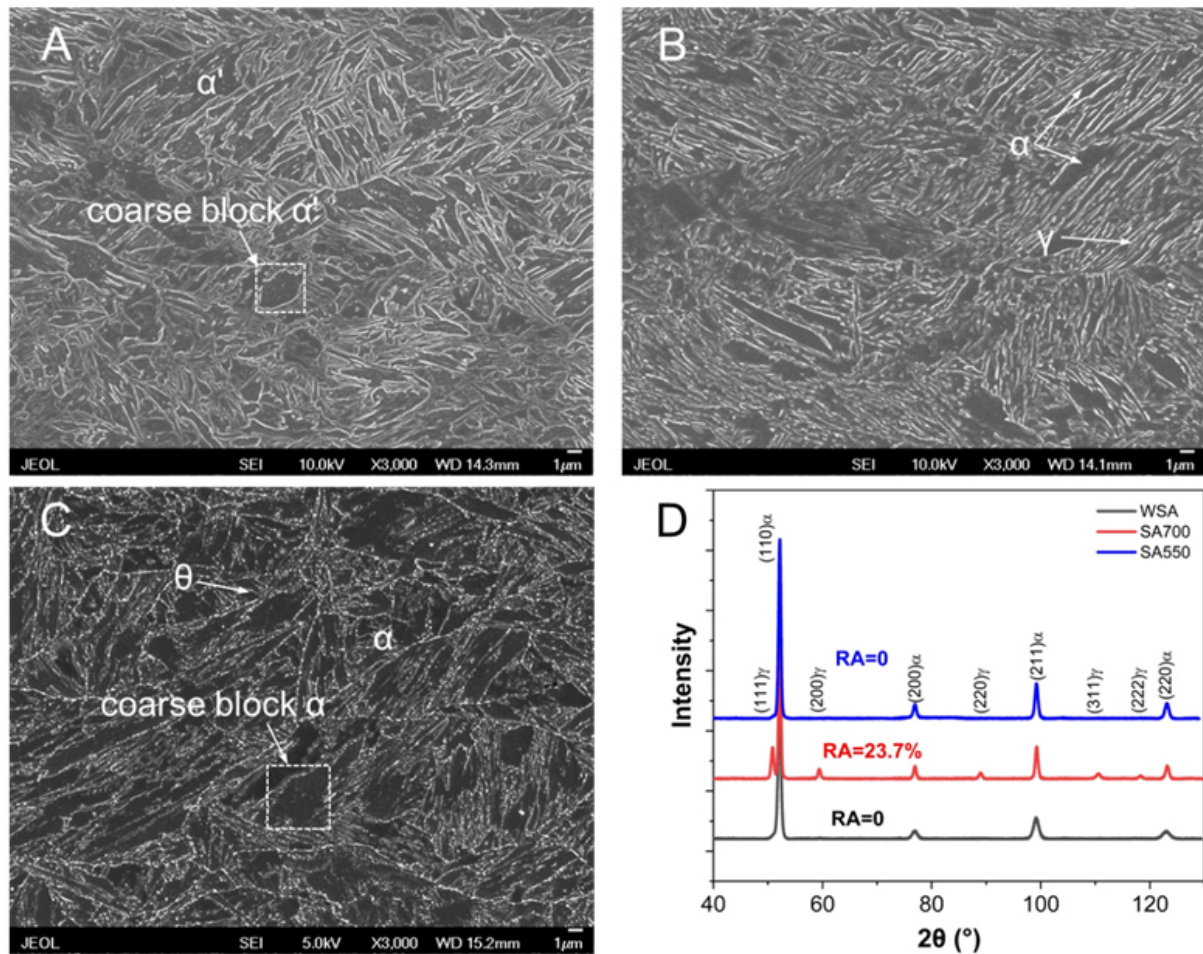


Figure 2. SEM micrographs of samples subjected to different SA processes: (A) WSA; (B) SA700; and (C) SA550. (D) X-ray diffraction patterns of the samples after different SA processes. α' , martensite; α , ferrite; γ , austenite; θ , cementite. SEM: Scanning electron microscope.

blocks in SA550 also do not have uniform sizes, which appears to inherit the characteristics of martensite in WSA since martensite was decomposed to ferrite and cementite during SA at 550 °C.

The cold-rolled microstructures and XRD results on the three samples after the CR are shown in [Figure 3](#). [Figure 3A](#) shows that the microstructure in WSA is still martensite but obviously elongated along the rolling direction. [Figure 3B](#) shows the severely deformed dual-phase microstructures of SA700 consisting of both ferrite and martensite, the latter transformed from austenite during cold rolling. In contrast, deformed ferrite and a large number of cementite particles were observed in SA550 [[Figure 3C](#)]. Since cementite particles are only formed at high angle boundaries, there are many more cementite particles in the region of elongated ultrafine ferrite grains than in the coarse ferrite grains, *i.e.*, the cementite particles do not distribute uniformly either.

[Figure 4A-C](#) shows the microstructures consisting of both ferrite and austenite formed in the three IA samples after the IA at 700 °C for 10 min. The XRD results in [Figure 4D](#) reveal that the RA fractions in these samples are almost the same as the equilibrium fraction of 29.3%, suggesting almost all intercritical austenite grains are retained and only a negligible amount of martensite formed during cooling. In addition to globular ferrite and austenite grains found in all samples, coarse ferrite bands (CFB) including some retained austenite grains were observed in WSA, while fine ferrite bands (FFB) without austenite appeared in SA550 and they resemble the elongated ferrite blocks after CR in [Figure 3C](#) except for cementite that had been almost completely dissolved. In contrast, both CFB and FFB are absent in SA700, where only the globular ultrafine ferrite and austenite grains were found.

[Figure 5](#) presents the EBSD results on the microstructures after IA at 700 °C for 10 min. The phase distribution overlapped with the image quality map is shown in [Figure 5A-C](#), while the grain boundary map is shown in [Figure 5D-F](#). It is seen that the CFB in WSA consists of several abnormal coarse ferrite grains, while the FFB in SA550 is large and elongated ferrite grains including many sub-boundaries. Moreover, there are fewer austenite grains in the CFB region than in the other regions of WSA - and even fewer austenite grains in the FFB regions of SA550. In contrast, they are uniformly distributed in the SA700 sample. [Figure 5G-I](#) provides the kernel average misorientation (KAM) mapping in these IA samples, which represents the density of geometry necessary dislocations that were produced near the phase interfaces due to the volume change accompanying phase transformation ^[21]. The KAM results reveal that both recovery and recrystallization could occur in all samples during IA at 700 °C for 10 min. The CFB region is the completely recrystallized region, while FFB is the recovered region. Moreover, the mean KAM value in the SA550 sample (0.823) is significantly higher than those in the WSA (0.648) and SA700 (0.665) samples, indicating the lowest degree of recrystallization.

Such different recrystallization behavior has also been reported elsewhere and attributed to the uneven stress distribution caused during deformation due to microstructural heterogeneity^[22,23]. To explore the exact mechanism in our work, the Mn concentration distribution in the hot-rolled plate was measured, as shown in [Figure 6](#). [Figure 6B](#) shows the slight but clear Mn chemical micro-bandings along the rolling direction after HR. This is usually due to the inevitable segregation of Mn during the solidification process^[24]. Such a compositional heterogeneity may not be sufficient to make the remarkable influence on the microstructural heterogeneity after the SA at 700 °C [[Figure 2B](#)], but the resultant influence, indeed, became significant after cold rolling. Since the high stored energy was accumulated during CR, the recrystallization and growth of ferrite grains may precede the reverse austenitic transformation in the Mn-lean regions during the heating or isothermal process due to the weaker solute drag effect and higher transformation temperature, leading to the formation of abnormal coarse ferrite grains [[Figure 4A](#)]. The measured Mn concentration distribution in WSA after the IA process also confirmed that the Mn concentration in the recrystallized region is relatively lower than the one in the recovered region [[Figure 7](#)].

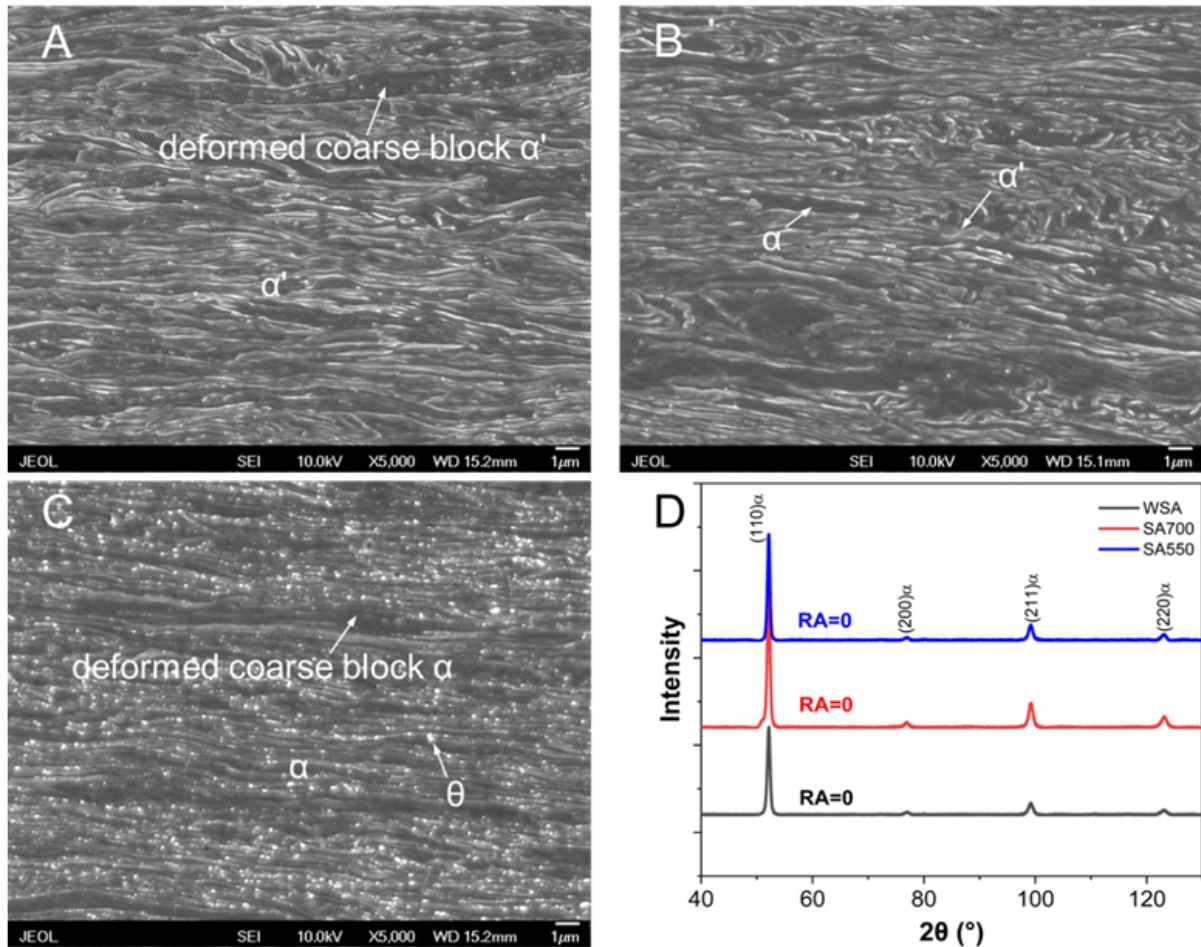


Figure 3. SEM micrographs of samples: (A) WSA; (B) SA700; and (C) SA550. (D) X-ray diffraction patterns of all samples after cold rolling. SEM: Scanning electron microscope.

The overall microstructural evolution is illustrated in Figure 8. The hot-rolled microstructure is fully martensitic, including Mn-segregated bands and martensite blocks of various sizes. After the different SA processes, austenite and ferrite are almost uniformly distributed in the SA700 sample because the temperature of 700 °C is high enough to weaken the influence of initial Mn segregation so that the reverse austenitic transformation could occur almost everywhere during SA at 700 °C. During CR, all the grains were elongated along the rolling direction, austenite transformed to martensite in SA700, but cementite in SA550 remained non-deformed. During the subsequent IA process, cold-deformed ferrite grains recrystallized and then grew more adequately in the Mn-lean regions of WSA sample before the reverse transformation due to higher transformation temperature than elsewhere, leading to the formation of CFB. Since deformation-induced martensite has a higher density of dislocations and higher C/Mn concentrations than ferrite in SA700, it acts as the nucleation site for austenitization during IA, leading to nearly uniformly distributed austenite and ferrite grains since the latter's growth is restrained by the formed austenite grains^{125]}. The cementite particle formed during SA at 550 °C, on the one hand, provided the nucleation sites for austenitization and, on the other hand, suppressed recrystallization, leading to the highest KAM value in SA550 after IA [Figure 5]. The FFB region in SA550 resulted from the coarse martensite blocks in the hot-rolled structure, where no cementite precipitated during SA at 550 °C due to the lack of high angle grain boundaries. The cold-rolled ferrite grains in this region were recovered during IA, forming FFB in SA550.

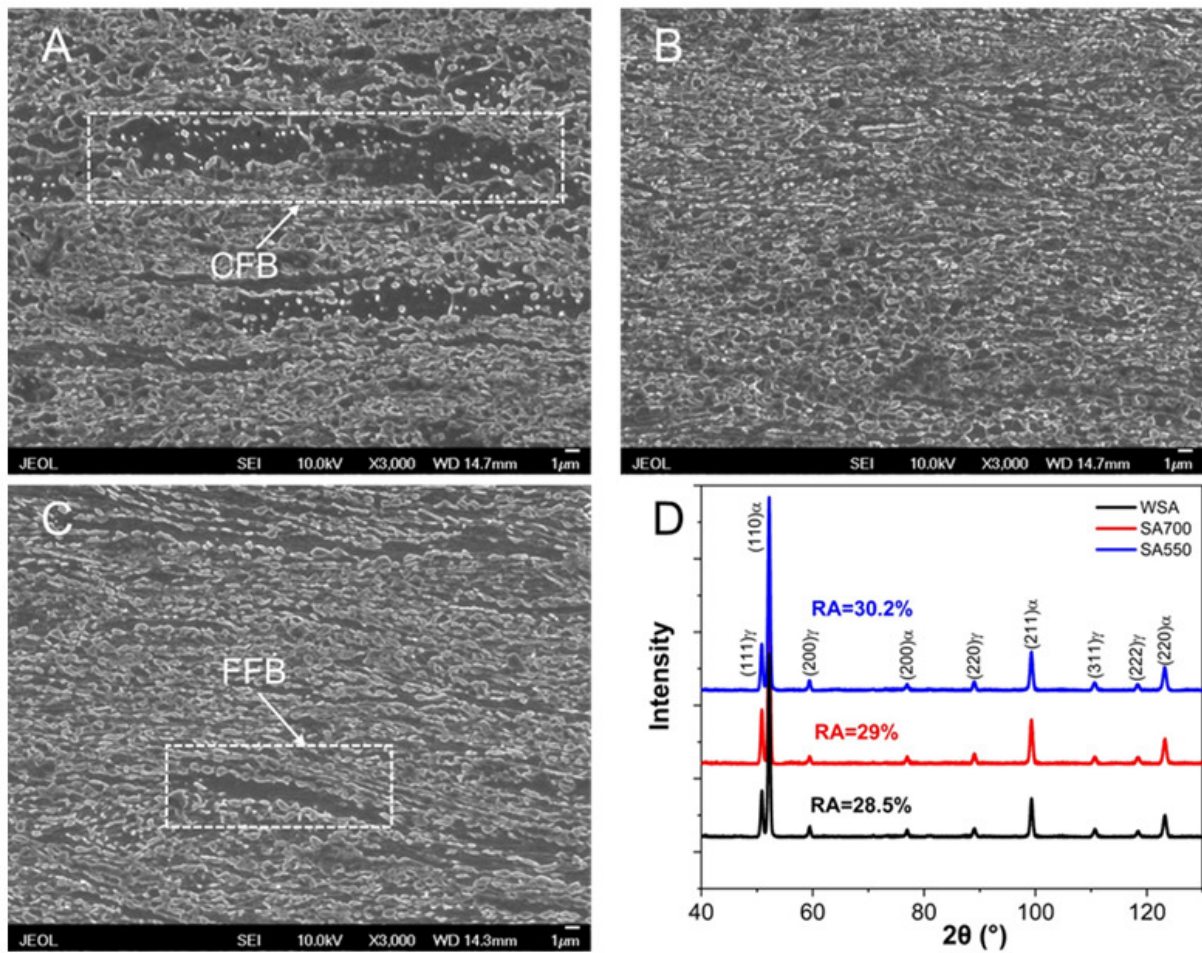


Figure 4. SEM micrographs of samples after IA at 700 °C for 10 min: (A) WSA; (B) SA700; and (C) SA550. (D) X-ray diffraction patterns of the IA samples. SEM: Scanning electron microscope.

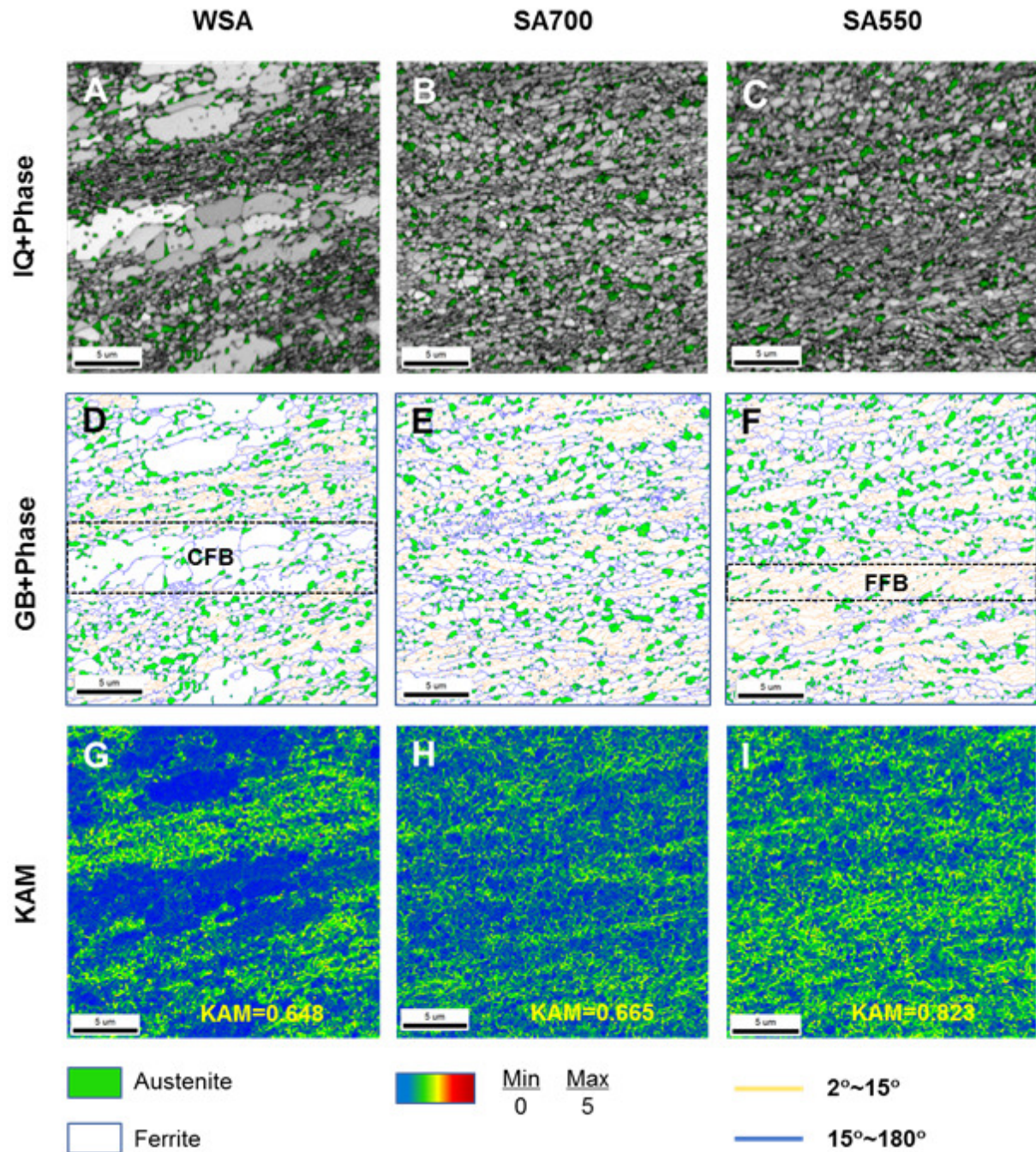


Figure 5. EBSD examination of samples after IA at 700 °C for 10 min: (A,D,G) WSA; (B,E,H) SA700; and (C,F,I) SA550. (A-C) The phase distribution overlapped with IQ map; (D-F) the phase distribution overlapped with grain boundary map, where the blue and orange lines represent the high (15°-180°) and low (2°-15°) angle boundaries, respectively; and (G-I) KAM mapping. EBSD: Electron backscattering diffraction; IA: intercritical annealing; SA: softening annealing; IQ: image quality; KAM: kernel average misorientation.

The size of FFB in SA550 is smaller than that of CFB in WSA because the cementite particles outside of this region could inhibit the growth of ferrite grains^[26]. Moreover, few austenite grains were formed in FFB because almost no cementite particles or high angle grain boundaries were available to act as the nucleation site of austenite, as shown in [Figure 5](#).

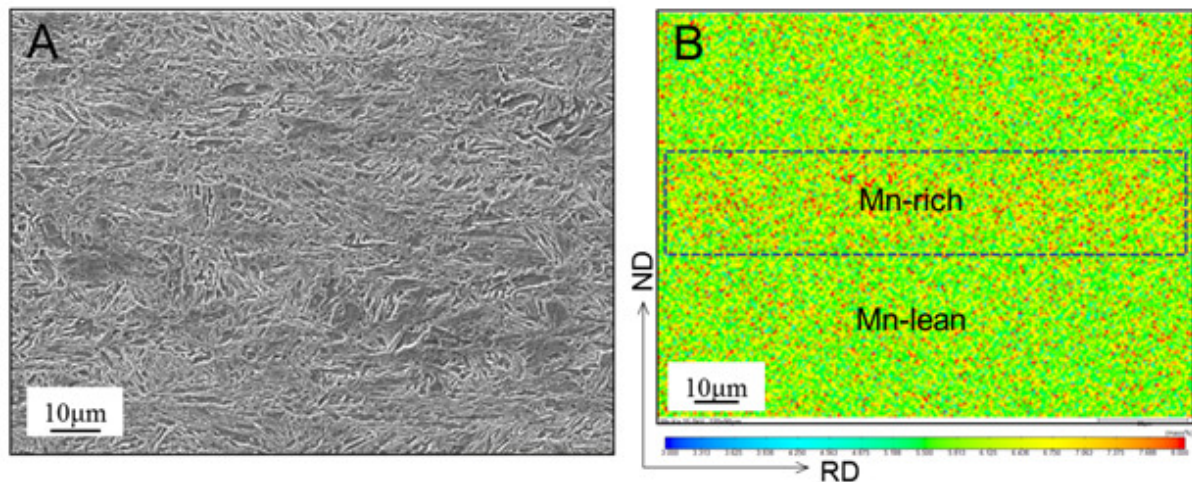


Figure 6. (A) Secondary electron contrast micrograph and (B) EPMA Mn distribution map in the hot-rolled plate. ND: Normal direction; RD: rolling direction; EPMA: electron probe microanalysis.

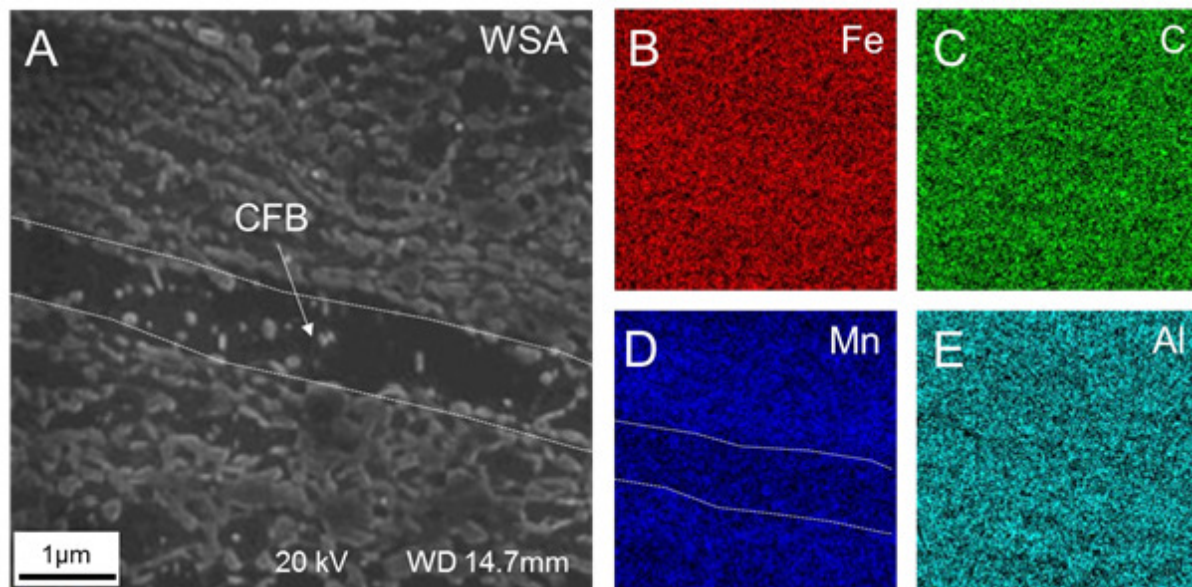


Figure 7. (A) SEM micrograph. SEM-EDS elementary mappings of the WSA sample after the IA at 700 °C for 10 min: (B) Fe; (C) C; (D) Mn; and (E) Al. SEM: Scanning electron microscope; EDS: energy dispersive spectrometer; IA: intercritical annealing.

Figure 9A shows the engineering stress–strain curves for all samples after IA. All curves show significant yield drops and clear yield platforms, followed by apparent work hardening until fracture. The plateau results from strain localization in Lüders band that spreads across the gauge of the specimen during yielding, followed by the rapid multiplication of dislocation for work hardening. This is frequently observed in MMS and has been intensively researched recently^[27,28]. Yield strength (YS), ultimate tensile strength (UTS), total elongation (TE), and yield point elongation are compared for all specimens in Figure 9B, as well as listed in Table 1 together with the product of tensile strength and elongation (PSE). Compared with the WSA sample, YS and TE of SA700 and SA550 increased by about 75 and 69 MPa and 6.2% and 1.9%, respectively. In other words, the WSA sample exhibits the lowest YS, TE, and PSE, and SA700 has the highest PSE value due to its excellent plasticity.

Table 1. Mechanical properties of different samples after IA at 700 °C for 10 min

Sample	YS (MPa)	UTS (MPa)	TE (%)	YPE (%)	PSE (GPa %)
WSA	860 ± 10	1085 ± 15	20.8 ± 0.8	5.38 ± 0.15	22.5 ± 1.1
SA700	935 ± 3	1076 ± 11	27.0 ± 0.8	6.79 ± 0.29	29.0 ± 0.5
SA550	929 ± 9	1128 ± 9	22.6 ± 0.3	5.75 ± 0.45	25.5 ± 0.1

IA: Intercritical annealing; YS: yield strength; UTS: ultimate tensile strength; TE: total elongation; YPE: yield point elongation; PSE: product of tensile strength and elongation; SA: softening annealing.

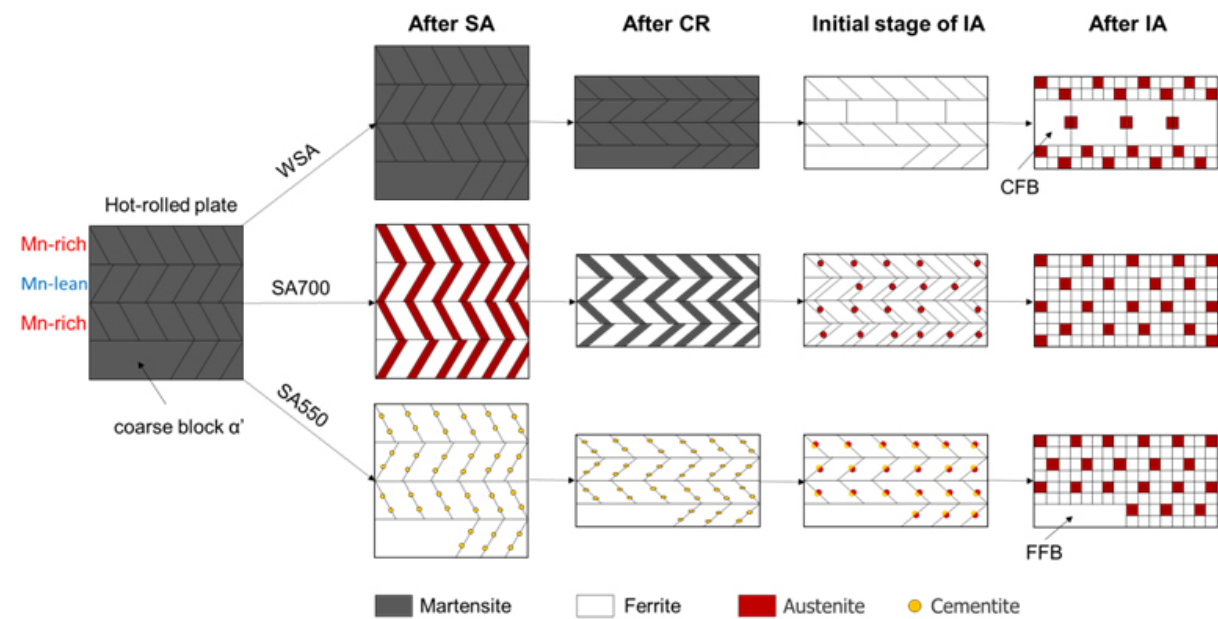


Figure 8. Schematic diagram of the microstructure evolution in the different processing routes of manufacturing WSA, SA700, and SA500 samples.

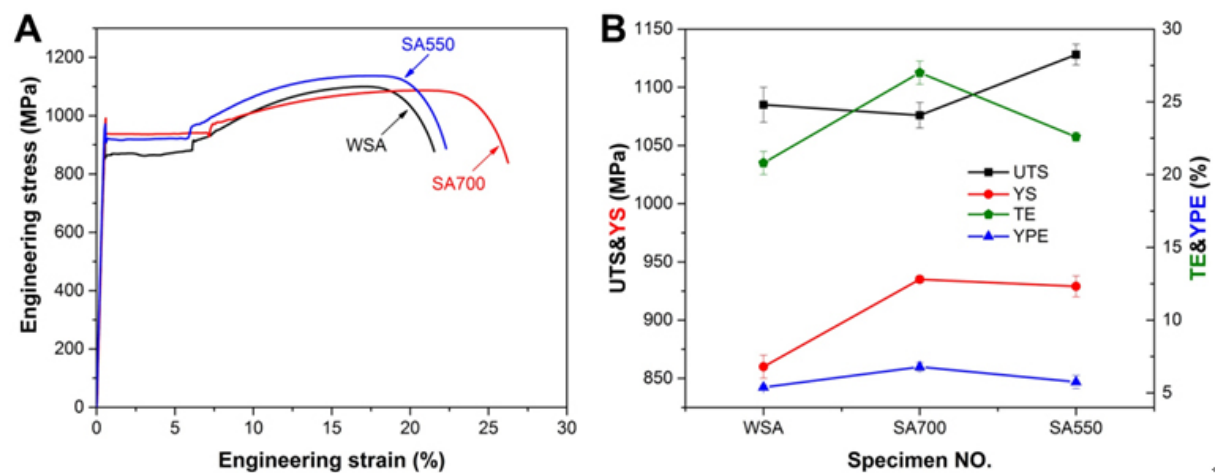


Figure 9. (A) Engineering stress-strain curves of different samples after the IA at 700 °C for 10 min. (B) Comparisons of YS, UTS, TE, and YPE between the IA samples. YS: Yield strength; UTS: ultimate tensile strength; TE: total elongation; IA: intercritical annealing; YPE: yield point elongation.

Although the ductility of MMS is often related to the fraction and stability of austenite, the RA fractions in the three samples after IA are similar, but the resultant ductility is different. The average grain sizes of austenite grains before deformation were also measured from the EBSD images [Figure 5] using Orientation Imaging Microscopy software. Due to the limited resolution, the fine grains with diameters below 100 nm were excluded for statistical analysis. The derived average values with standard deviations were plotted [Figure 10A], indicating that the RA grains in these specimens have similar sizes. The RA fractions measured after the tensile deformation by XRD indicate that almost all the austenite grains in these samples transformed to martensite during deformation [Figure 10B]. Moreover, interrupted tensile tests were conducted to study the mechanical stability of austenite, and the XRD results are shown in Figure 10C. Among all specimens, the smallest fraction of RA grain in WSA transformed to martensite during the tensile strain to 9%, suggesting that RA grains in WSA have the highest mechanical stability, probably because the RA grains located in CFB may contain the highest C content due to the strongest partition of C from the neighboring coarsest ferrite grains [Figure 5D]. In contrast, the RA grains in other specimens had similar stability as they transformed to similar fractions during deformation. Nevertheless, the WSA specimen exhibited the worst ductility [Figure 10C], indicating that the austenite phase should not be responsible for the different ductility measured in these samples.

Figure 11 shows the cracks propagating along the rolling direction in the WSA sample during tensile deformation. The crack propagated along the boundary between the CFB and ultrafine-grained dual-phase regions. The CFB region consists of abnormally coarse ferrite grains, which are relatively soft because of the complete recrystallization, limited number of grain boundaries, and low alloying contents. Therefore, cracks might be initiated and propagated along the boundary between them during deformation, where stress concentration was developed due to the different strain hardening capacities. It is concluded that microstructural heterogeneity is an important reason for the low elongation measured in WSA. In contrast, the FFB region in SA550 contains many sub-boundaries resulting from recovery, leading to higher strength and greater elongation than those of the WSA sample. In the SA700 sample, ferrite and austenite phases with an ultrafine size are evenly distributed so that the strain localization for the onset of necking due to the stress concentration was greatly delayed, leading to the best plasticity among all the specimens.

Figure 9 shows that YS of SA700 is the highest while WSA shows the lowest YS. It is generally accepted that yielding occurs firstly in the soft phase of MMS, *i.e.*, ferrite in our study, as discussed above. In this case, YS is closely related to the size of ferrite grains: the lowest YS due to the coarsest CFB in WSA and the highest YS due to the ultrafine ferrite grains in SA700 formed after the IA process.

Although the heterogeneous distribution of Mn resulting from Mn segregation cannot be avoided in MMS, it is still possible to achieve ultrafine dual-phase microstructures with homogenous distribution via introducing sufficient nucleation sites for the reverse transformation at a high enough annealing temperature, as seen in SA700. This can remove the banded structures resulting from the heterogenous Mn distribution, thus improving both elongation and yield strength. Therefore, this study hints at a new approach to improve the mechanical properties of MMS by utilizing the adverse effects of Mn segregation.

CONCLUSIONS

In this work, a medium Mn steel was manufactured via the hot rolling, softening annealing, cold rolling, and intercritical annealing process, in which only the softening annealing process was changed to investigate the microstructural heredity in the processing route and its influence on the resultant tensile properties.

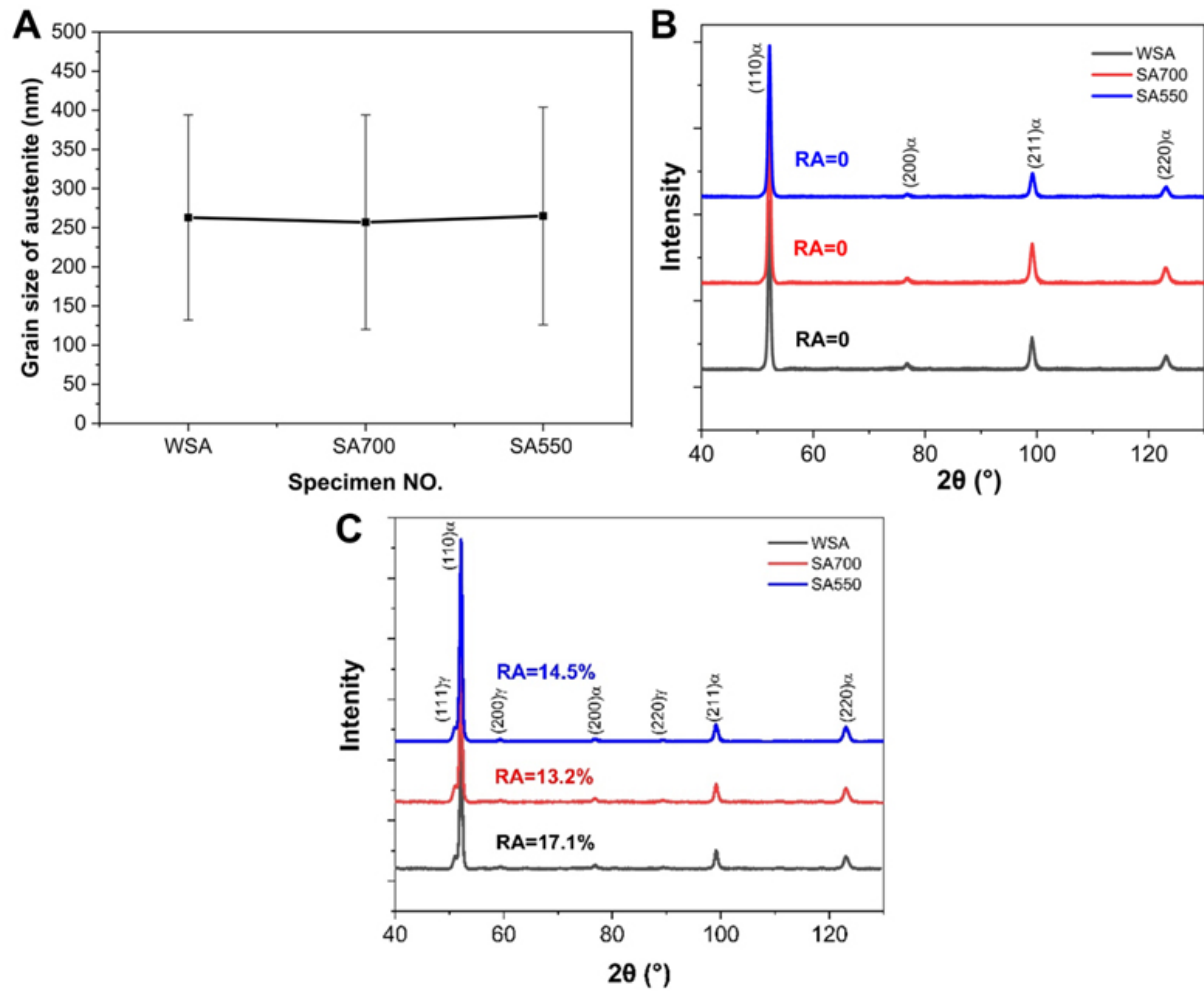


Figure 10. (A) The average grain size of austenite of different samples after IA at 700 °C for 10 min. (B) X-ray diffraction patterns of the different samples after tensile deformation. (C) X-ray diffraction patterns of the interrupted samples when the strain is 9%. IA: Intercritical annealing.

(a) In the case of no softening annealing employed, both recrystallization and growth of ferrite grains may precede the reverse austenitic transformation in the Mn-lean regions during IA due to the weaker solute drag effect and higher transformation temperature, leading to the formation of abnormal coarse ferrite grains that deteriorated ductility due to the cracking propagated along the boundary of the coarse-grained and fine-grained regions.

(b) When the softening annealing was performed at 700 °C, which is much higher than the temperatures for both cementite to dissolve and austenite to appear during heating, the uniformly distributed austenite grains were formed and later transformed to martensite during cold rolling; the dislocated martensite is the uniformly distributed nucleation sites for austenitization during the subsequent IA, resulting in ultrafine-grained ferrite-plus-austenite dual-phased microstructures for improving ductility.

(c) When martensite was annealed at 550 °C, it decomposed to ferrite and cementite; the latter not only significantly inhibited recrystallization but also promoted the nucleation of austenite during the subsequent IA. However, the resultant austenite grains are not as uniformly distributed as those in SA700 because

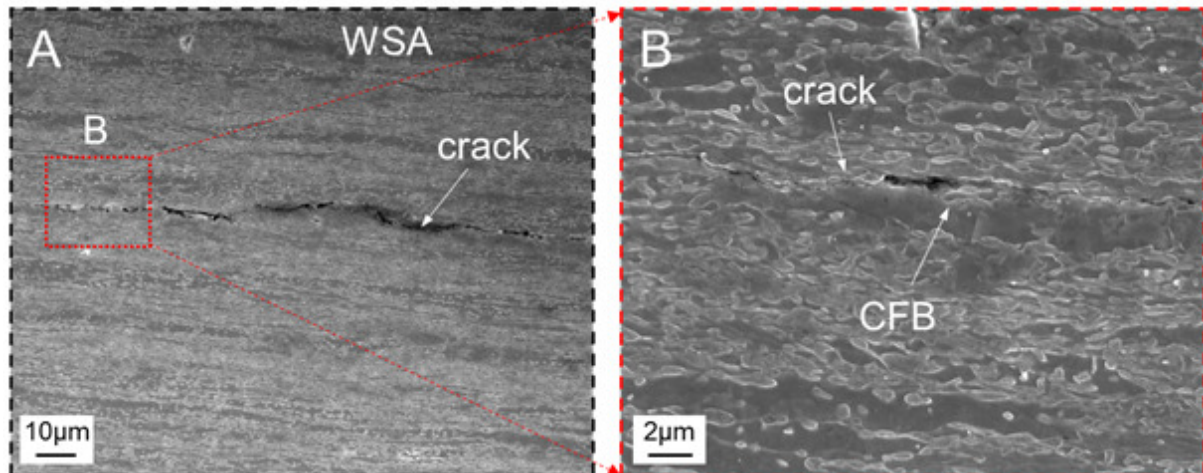


Figure 11. (A) SEM micrograph of cracks along the rolling direction. (B) The local enlarged image of the WSA sample after a tensile fracture. SEM: Scanning electron microscope.

cementite particles mainly precipitated at high angle boundaries, leading to inferior ductility compared to SA700.

DECLARATIONS

Authors' contributions

Design: Hu B

Experiments: Ding F

Data analysis: Guo Q, Hu B

Manuscript writing: Guo Q, Ding F

Manuscript revision and supervising: Luo H

Availability of data and materials

Not applicable.

Financial support and sponsorship

H.W. Luo acknowledges the financial support from National Natural Science Foundation of China (No. 51831002). B. Hu acknowledges the National Natural Science Foundation (No. 51904028), Fundamental Research Funds for the Central Universities (Nos. FRF-TP-18-002C2, 06600019, 06500151).

Conflicts of interest

All authors declared that there are no conflicts of interest.

Ethical approval and consent to participate

Not applicable.

Consent for publication

Not applicable.

Copyright

© The Author(s) 2021.

REFERENCES

1. Yang D, Du P, Wu D, Yi H. The microstructure evolution and tensile properties of medium-Mn steel heat-treated by a two-step annealing process. *Journal of Materials Science & Technology* 2021;75:205-15. DOI
2. Li X, Song R, Zhou N, Li J. An ultrahigh strength and enhanced ductility cold-rolled medium-Mn steel treated by intercritical annealing. *Scripta Materialia* 2018;154:30-3. DOI
3. Zhang X, Yan J, Liu T, et al. Microstructural evolution and mechanical behavior of a novel heterogeneous medium Mn cold-rolled steel. *Materials Science and Engineering: A* 2021;800:140344. DOI
4. Aydin H, Essadiqi E, Jung I, Yue S. Development of 3rd generation AHSS with medium Mn content alloying compositions. *Materials Science and Engineering: A* 2013;564:501-8. DOI
5. Chiang J, Lawrence B, Boyd J, Pilkey A. Effect of microstructure on retained austenite stability and work hardening of TRIP steels. *Materials Science and Engineering: A* 2011;528:4516-21. DOI
6. Gibbs PJ, De Moor E, Merwin MJ, Clausen B, Speer JG, Matlock DK. Austenite Stability Effects on Tensile Behavior of Manganese-Enriched-Austenite Transformation-Induced Plasticity Steel. *Metall and Mat Trans A* 2011;42:3691-702. DOI
7. Han J, Lee Y. The effects of the heating rate on the reverse transformation mechanism and the phase stability of reverted austenite in medium Mn steels. *Acta Materialia* 2014;67:354-61. DOI
8. Cai Z, Ding H, Misra R, Ying Z. Austenite stability and deformation behavior in a cold-rolled transformation-induced plasticity steel with medium manganese content. *Acta Materialia* 2015;84:229-36. DOI
9. Chiang J, Boyd J, Pilkey A. Effect of microstructure on retained austenite stability and tensile behaviour in an aluminum-alloyed TRIP steel. *Materials Science and Engineering: A* 2015;638:132-42. DOI
10. Hu B, Luo H. A novel two-step intercritical annealing process to improve mechanical properties of medium Mn steel. *Acta Materialia* 2019;176:250-63. DOI
11. Jang J, Kim S, Kang NH, Cho K, Suh D. Effects of annealing conditions on microstructure and mechanical properties of low carbon, manganese transformation-induced plasticity steel. *Met Mater Int* 2009;15:909-16. DOI
12. Lee S, Lee S, De Cooman BC. Austenite stability of ultrafine-grained transformation-induced plasticity steel with Mn partitioning. *Scripta Materialia* 2011;65:225-8. DOI
13. Han J, Lee S, Jung J, Lee Y. The effects of the initial martensite microstructure on the microstructure and tensile properties of intercritically annealed Fe-9Mn-0.05C steel. *Acta Materialia* 2014;78:369-77. DOI
14. Li Z, Wang T, Zhang X, Zhang F. Annealing softening behaviour of cold-rolled low-carbon steel with a dual-phase structure and the resulting tensile properties. *Materials Science and Engineering: A* 2012;552:204-10. DOI
15. Benzing JT, Luecke WE, Mates SP, Ponge D, Raabe D, Wittig JE. Intercritical annealing to achieve a positive strain-rate sensitivity of mechanical properties and suppression of macroscopic plastic instabilities in multi-phase medium-Mn steels. *Mater Sci Eng A Struct Mater* 2021;803:140469. DOI PubMed PMC
16. Wu Y, Sun W, Styles M, Arlazarov A, Hutchinson C. Cementite coarsening during the tempering of Fe-C-Mn martensite. *Acta Materialia* 2018;159:209-24. DOI
17. Yan S, Liu X, Liang T, Zhao Y. The effects of the initial microstructure on microstructural evolution, mechanical properties and reversed austenite stability of intercritically annealed Fe-6.1Mn-1.5Si-0.12C steel. *Materials Science and Engineering: A* 2018;712:332-40. DOI
18. Luo H, Dong H, Huang M. Effect of intercritical annealing on the Lüders strains of medium Mn transformation-induced plasticity steels. *Materials & Design* 2015;83:42-8. DOI
19. Ding R, Dai Z, Huang M, et al. Effect of pre-existed austenite on austenite reversion and mechanical behavior of an Fe-0.2C-8Mn-2Al medium Mn steel. *Acta Materialia* 2018;147:59-69. DOI
20. Cao W, Wang C, Shi J, Wang M, Hui W, Dong H. Microstructure and mechanical properties of Fe-0.2C-5Mn steel processed by ART-annealing. *Materials Science and Engineering: A* 2011;528:6661-6. DOI
21. Li S, Wen P, Li S, Song W, Wang Y, Luo H. A novel medium-Mn steel with superior mechanical properties and marginal oxidation after press hardening. *Acta Materialia* 2021;205:116567. DOI
22. Sarkar A, Sanyal S, Bandyopadhyay TK, Mandal S. Recrystallization behaviour and tensile properties of Al-added medium-Mn-steel at different deformation-annealing conditions. *Materials Science and Technology* 2018;35:2054-68. DOI
23. Zheng C, Raabe D. Interaction between recrystallization and phase transformation during intercritical annealing in a cold-rolled dual-phase steel: A cellular automaton model. *Acta Materialia* 2013;61:5504-17. DOI
24. Jo MC, Lee H, Zargarani A, et al. Exceptional combination of ultra-high strength and excellent ductility by inevitably generated Mn-segregation in austenitic steel. *Materials Science and Engineering: A* 2018;737:69-76. DOI
25. Yang DZ, Brown EL, Matlock DK, Krauss G. Ferrite recrystallization and austenite formation in cold-rolled intercritically annealed steel. *MTA* 1985;16:1385-92. DOI
26. Zhu Y, Hu B, Luo H. Influence of Nb and V on Microstructure and Mechanical Properties of Hot-Rolled Medium Mn Steels. *steel research int* 2018;89:1700389. DOI
27. Sun B, Ma Y, Vanderesse N, et al. Macroscopic to nanoscopic in situ investigation on yielding mechanisms in ultrafine grained medium Mn steels: Role of the austenite-ferrite interface. *Acta Materialia* 2019;178:10-25. DOI
28. Hu B, Ding F, Tu X, et al. Influence of lamellar and equiaxed microstructural morphologies on yielding behaviour of a medium Mn steel. *Materialia* 2021;20:101252. DOI